# Full-scale Development of Novel Vapor Chambers for Heating and Cooling of Carbon Dioxide Adsorbent System

Elizabeth K. Seber<sup>1</sup>, Giovanina Bell<sup>2</sup>, and Ion Nicolaescu<sup>3</sup> *Advanced Cooling Technologies, Lancaster, Pennsylvania, 17601* 

The Four-Bed Carbon Dioxide Scrubber (4BCO<sub>2</sub>) is a next-generation CO<sub>2</sub> removal system developed to improve upon the legacy Carbon Dioxide Removal Assembly (CDRA) by efficiently removing carbon dioxide from the spacecraft cabin atmosphere. Unlike the CDRA, which vents the captured CO2 as waste, the 4BCO2 delivers a concentrated CO2 stream suitable for downstream utilization. One key application is oxygen recovery via the Sabatier reactor, which converts CO2 and hydrogen into water and methane. In earlier life support architectures, this CO2 stream required a separate mechanical compressor to achieve the pressure levels necessary for Sabatier operation. To reduce system complexity, power consumption, and mass, the newly developed Air-Cooled Temperature Swing Adsorption Compressor (AC-TSAC) was introduced as a replacement for the mechanical compressor. The AC-TSAC combines adsorption-based CO<sub>2</sub> compression with integrated thermal swing regeneration to produce a pressurized CO2 output, suitable for direct use in onboard processing systems. A critical challenge in the 4BCO<sub>2</sub> system is the efficient regeneration of zeolite sorbent beds, which must be heated from ambient (~20 °C) to over 220 °C despite the material's low thermal conductivity (~0.13 W/m·K). To overcome this limitation, the sorbent beds have been redesigned to incorporate concentric vapor chambers-passive, two-phase thermal transport devices with high effective thermal conductivity and near-isothermal performance. This work presents the design, optimization, and fabrication of vapor chamberintegrated 4BCO<sub>2</sub> beds, including wick design, thermal modeling, and additive manufacturing approaches.

## **Acronyms and Nomenclature**

 $4BCO2 = 4-Bed\ CO2\ scrubber$ 

A = Area

ACT = Advanced Cooling Technologies, Inc.

AC-TSAC = Air-Cooled, Temperature Swing Adsorption Compressor

 $\alpha$  = Thermal Diffusivity AM = Additive Manufacturing

Bi = Biot Number

*CDRA* = Carbon Dioxide Removal Assembly

 $CO_2$  = Carbon Dioxide  $\Delta P$  = Change in Pressure

 $\Delta P_c$  = Capillary Pressure Difference  $\Delta T$  = Change in Temperature dx = Change in Length (x) Fo = Fourier Number g = Gravitational Constant

*h* = Surface Convection Coefficient

 $h_c$  = Heat Transfer Coefficient of Condensation

 $h_{fg}$  = Latent Heat Capacity

K = Permeability

<sup>&</sup>lt;sup>1</sup> R&D Engineer II, R&D Department, 1046 New Holland Avenue, Lancaster, PA 17601.

<sup>&</sup>lt;sup>2</sup> R&D Intern, R&D Department, 1046 New Holland Avenue, Lancaster, PA 17601.

<sup>&</sup>lt;sup>3</sup> Senior R&D Engineer, R&D Department, 1046 New Holland Avenue, Lancaster, PA 17601.

k = Thermal Conductivity LPBF = Laser Powder Bed Fusion  $L_c$  = Characteristic Length  $\mu$  = Liquid Viscosity

 $\dot{Q}_{Actual}$  = Actual Applied Heat Load

 $\dot{Q}_{Analogy}$  = Heat Load used in the Thermal-Flow Analogy

 $r_e$  = Effective Radius

 $\rho$  = Density

 $\sigma$  = Surface Tension

t = Time

TC = Thermocouple  $\theta$  = Wetting Angle  $\dot{V}$  = Volumetric Flow Rate VC = Vapor Chamber

#### I. Introduction

In space habitats, environmental controls are a crucial component for every manned mission, from short space walks to extraterrestrial stations. In survival guides, the rule of threes is a shorthand method of understanding what the needs and limitations are for humans. The average human can survive approximately three weeks without food, three days without drinkable water, and only three minutes without oxygen. With how dire the need for breathable air is in the vacuum of space, there are several systems needed for providing and conditioning the air. Carbon dioxide (CO<sub>2</sub>) removal is a major component of the environmental controls, as without it, carbon dioxide can build up within the space habitat to dangerously high levels.

The Carbon Dioxide Removal Assembly (CDRA) is the legacy CO<sub>2</sub> removal system used aboard the International Space Station (ISS). In this system, zeolite sorbent beds capture CO<sub>2</sub> from the cabin air. To regenerate the beds, the CO<sub>2</sub>-rich chamber is isolated, heated from approximately 20 °C to 200 °C<sup>2</sup>, and subjected to vacuum to desorb the captured CO<sub>2</sub>. The newer Four-Bed Carbon Dioxide Scrubber (4BCO<sub>2</sub>) system improves upon CDRA by capturing CO<sub>2</sub> more efficiently and delivering a concentrated CO<sub>2</sub> stream suitable for downstream processing. Previously, this low-pressure stream required a separate mechanical compressor to feed into the Sabatier reactor for oxygen recovery. To address this limitation, the newly developed Air-Cooled Temperature Swing Adsorption Compressor (AC-TSAC) was introduced. The AC-TSAC pressurizes CO<sub>2</sub> during the desorption phase, delivering a steady, high-pressure stream directly to the Sabatier reactor, where it is converted into water to support crew needs. Unlike CDRA and 4BCO<sub>2</sub>, which provide CO<sub>2</sub> at low pressure, the AC-TSAC integrates both CO<sub>2</sub> capture and compression into a single unit, significantly reducing the mass, volume, and complexity of the spacecraft's Environmental Control and Life Support System (ECLSS) architecture.

A major challenge to the design and implementation of the aforementioned CO<sub>2</sub> removal systems is tied to the sorbent material: zeolite. In order to release the captured CO<sub>2</sub> from the zeolite, the material must be raised in temperature up to 200 °C. Zeolite, however, has very low thermal conductivity (approximately 0.13 W/m•K)<sup>3</sup>, and so a robust thermal management system is needed to uniformly increase the temperature of the zeolite without overheating the zeolite to the point of burning.

Suggested thermal solutions involve the use of various embedded heaters. This includes cartridge heaters with axial fin structures, and more novelly, resistive wire heaters embedded in additively manufactured zeolite lattice structures.<sup>4</sup> This approach offers several benefits, however, a degree of durability is lost with the internally placed resistive heaters. Should the heaters be overpowered, there is a large risk of damaging the zeolite material. A broken internal heater cannot be easily replaced, which would result in loss of CO<sub>2</sub> capture and desorption capacity.

In this paper, a series of concentric circle-shaped vapor chambers are explored as a solution to this thermal challenge, building off of previous design efforts involving novel, star-shaped vapor chambers. Vapor chambers are passive heat transfer devices that rely on two-phase heat transport to carry large thermal loads. Due to the nature of two-phase heat transfer, they are also highly isothermal. This isothermality is ideal for uniformly heating the zeolite bed. Vapor chambers can transport heat over a considerable distance, which allows the heat source to be attached to the portion of the vapor chambers that are external to the zeolite bed. Concentric vapor chambers were selected due to their uniform symmetry within the cylindrical zeolite bed. An example of how the 4BCO2 bed may look with concentric vapor chambers is shown in Figure 1.

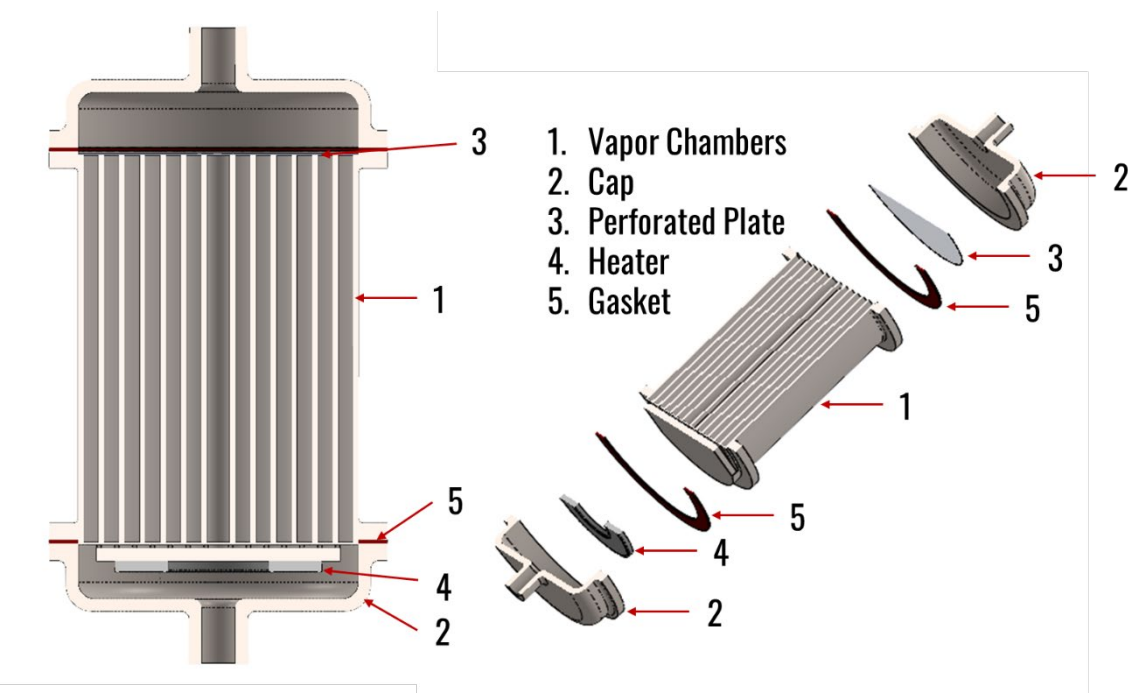


Figure 1. Cross-Sectional View of a 4BCO2 Bed with Concentric Vapor Chambers.

## **II.** Concentric Vapor Chambers

## A. Concentric Circle-Shaped Vapor Chambers

A transient thermal conduction model was created to determine how many vapor chambers were needed and the spacing of the vapor chambers. This analytical model first starts with some given definitions, such as zeolite material properties and the capture bed's dimensions. The interior volume of the CO<sub>2</sub> Capture bed is described as 12 inches in length, and 8 inches in diameter for a cylindrical bed.

Within the bed geometry, there exists a level of symmetry between each of the vapor chambers, and within the zeolite sections, as shown in Figure 2. With this, the bed with its many layers of zeolite and vapor chambers can be simplified into a single half section of zeolite, and a single half section of a vapor chamber. For this analytical model, this simplified geometry can be treated as an infinite plane wall, as the height of the bed is far greater than the relative characteristic length of the conduction path.

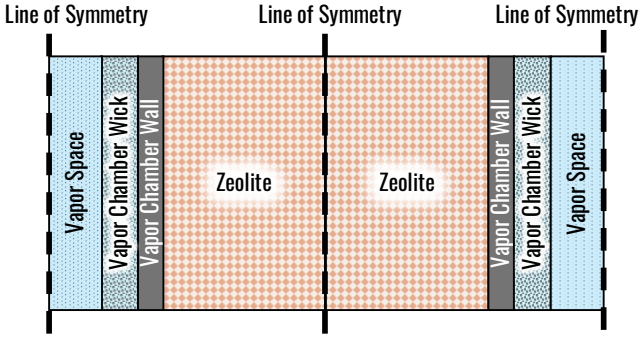


Figure 2. Schematic showing Lines of Symmetry that bisect both the zeolite sections, and the vapor chambers.

The Biot number (Bi) is a dimensionless coefficient that is used for thermal conduction calculations that also include surface convection. This value, as defined in Eq. (1), quantifies the surface convection coefficient (h), some characteristic length  $(L_c)$ , and the thermal conductivity (k) of the solid material. For this example, the vapor space and the condensation occurring on the wick is treated as the convection coefficient. The Biot number for the vapor chamber wall and wick is less than 0.1, and therefore for this model, the temperature across the vapor chamber is treated as

isothermal. Conversely, the Biot number for the zeolite is far greater than one, and so the lumped sum capacitance simplification cannot be used.

$$Bi = \frac{h \cdot L_c}{k} \tag{1}$$

The dimensionless time coefficient, known as the Fourier number (Fo), is paired with the Biot number for characterizing and solving transient conduction problems. The Fourier number in Eq. (2) is expressed in terms of thermal diffusivity ( $\alpha$ ), time (t), and the characteristic length.

$$Fo = \frac{\alpha \cdot t}{L_c^2} \tag{2}$$

The characteristic length is equal to one half of the zeolite section thickness. In this model, this length is the variable used to determine the spacing of the vapor chambers. This is the variable to solve for, such that after 10 minutes of continuous heating, the temperature at the centerline radius of the zeolite section reaches 200 °C. Using the Biot and Fourier numbers, an initial temperature of 20 °C, and a vapor chamber operating temperature of 230 °C, the transient model determined that seven vapor chambers, of thickness 0.15 in., spaced 0.459 in. apart would bring the minimum temperature of the bed up to 208.9 °C in the prescribed time of 10 minutes. This time requirement is set by the operational design of the AC-TSAC.

The thermal solution must raise the temperature of zeolite from room temperature (approximately  $20\,^{\circ}\text{C}$ ) to at least  $200\,^{\circ}\text{C}$  to release  $CO_2$  from the zeolite. Additionally, the zeolite must not exceed a maximum temperature of  $230\,^{\circ}\text{C}$  to prevent thermal degradation. Subtracting the volume of the vapor chambers from the volume of the bed, the remaining volume can be used to determine the quantity of zeolite. From there, the maximum thermal energy needed to raise that quantity of zeolite from  $20^{\circ}$  to at least  $200\,^{\circ}\text{C}$  can be calculated. This was determined to be  $2.1\,^{\circ}\text{MJ}$ . Given the time requirement of reaching  $200\,^{\circ}\text{C}$  in  $10\,^{\circ}$  minutes, the total power needed to raise that quantity of zeolite in temperature was determined to be  $3.532\,^{\circ}\text{kW}$ . To verify the results of this transient thermal conduction analysis, an FEA analysis was run on a simplified CAD model (Figure 3) of the array of concentric, circle-shaped vapor chambers. In this model, the vapor chambers are modeled as a boundary condition on the edges of the zeolite bed sections through a constant temperature ( $230\,^{\circ}\text{C}$ ) and a Total Heat Load ( $3.532\,^{\circ}\text{kW}$ ). The material properties of the zeolite for this model were determined from known zeolite properties and an anticipated packing porosity of 0.675. The zeolite was set with an initial temperature of  $20\,^{\circ}\text{C}$ .

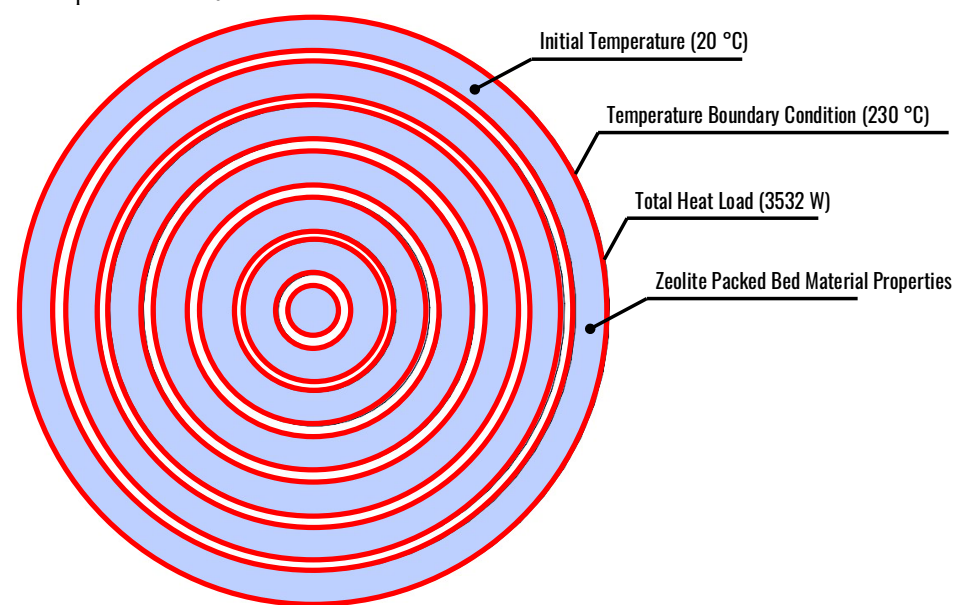


Figure 3. Simple CAD Model of the Zeolite Volume for Transient FEA Conduction Simulation

The temperature map of this simulation at 10 minutes is shown in Figure 4. Within each of the sectional "rings" of zeolite material, there is a symmetry about the centerline radius. The centerline temperature for each of these rings

is very close to the calculated, anticipated value of 208.9 °C. This is a good indication that the infinite plane wall assumption was valid for use in the analytical model. There is one exception, which is in the centermost volume of zeolite. Here, the radius of the material is too small for the infinite plane wall assumption, and the lowest temperatures in the model are seen at the very center of the zeolite bed (206 °C).

In this model, there is a large temperature gradient from the walls of the vapor chamber and the center of the zeolite section ( $\sim$ 20 °C) due to the large thermal resistance of the zeolite. While this arrangement of vapor chambers meets the goal of raising the minimum temperature of the zeolite to approximately 200 °C within 10 minutes, as required by the cyclic operation of the AC-TSAC, the temperature gradient could be improved by decreasing the spacing between the vapor chambers. However, doing so would result in volume taken from the zeolite to be supplied to the vapor chambers.

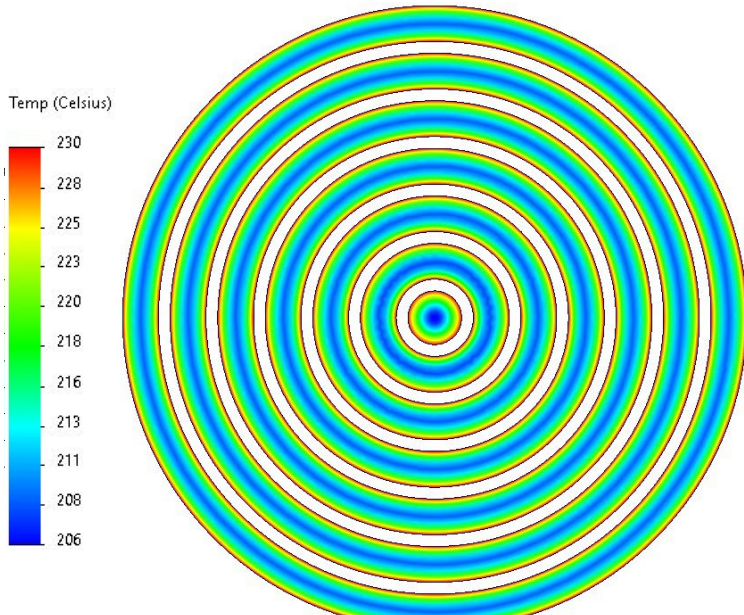


Figure 4. Temperature map of conduction through the concentric circle shaped vapor chamber zeolite bed.

## **B.** Arc-Shaped Vapor Chambers

In a previous design study that focused on a subscale zeolite bed, 6 design efforts found that the concentric vapor chambers could be separated into arc-shaped vapor chambers while maintaining the same degree of improved thermal performance. This change also increased the volume of the bed dedicated to zeolite instead of the volume dedicated to the thermal solution, improving the CO<sub>2</sub> capture efficiency of the system. To apply this to the full-scale zeolite bed, each concentric circle vapor chamber was separated into four arc-shaped vapor chambers, with the distance between each arc equal to the characteristic length identified as the zeolite section thickness. The exception for this is the centermost ring of vapor chambers, where the length between vapor chamber segments was reduced to ½ the characteristic length. The same boundary and material conditions from the concentric circle model were applied in this model, except for the total heat load, which was increased to accommodate for the additional zeolite material. The temperature map of conduction through the zeolite bed with arc-shaped vapor chambers is shown in Figure 5. After 10 minutes, the most notable temperature gradient is now in the space between vapor chambers with the same centerline radius, and the centermost region. For the centermost region, some optimization may yet be completed.

A summary of the thermal conduction results is provided in Table 1. The total volume of the bed for both models is 9.89 L. While the arch-shaped vapor chambers leave more room for zeolite, and therefore increase the CO<sub>2</sub> capture capacity of the bed, the average temperature and minimum of the bed is lower than the concentric-circle vapor chambers. This indicates poorer thermal performance. In selecting between the two designs, the concentric circle model offers the added benefit of lower complexity, with only seven circular vapor chambers compared to twenty-five arc-shaped vapor chambers. The complex assembly and sealing process of so many components makes the arc-shaped vapor chamber model less desirable. The authors will be using the concentric vapor chamber model moving forward in the design process.

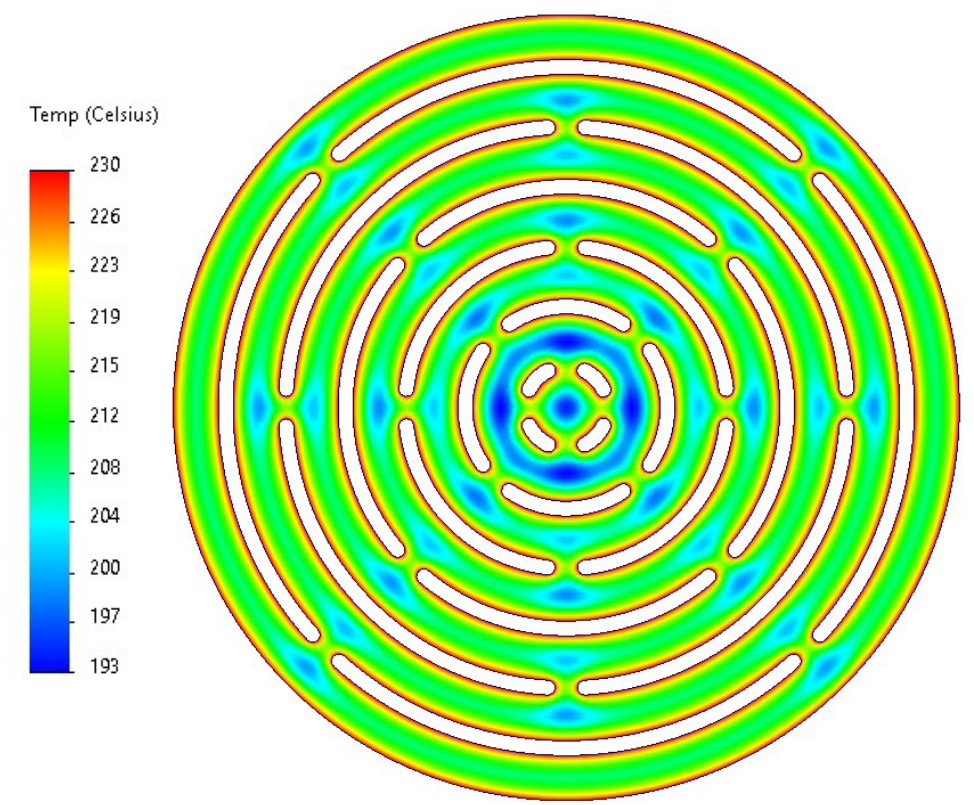


Figure 5. Temperature Map of Conduction Through a Full-Scale Zeolite Bed with Arc-Shaped Vapor Chambers after 10 minutes.

Table 1. Comparison of thermal model results.

Vapor Chamber Model	Heat Load [kW]	Volume of Zeolite [L]	Volume of Vapor Chambers [L]	Average Temperature at 10 Minutes [°C]	Minimum Temperature at 10 Minutes [°C]
Concentric Circles	3.534	7.72	2.17	214	206
Arc-Shaped	3.69	8.06	1.82	212	193

## III. Wick Design Study

#### A. Additively Manufactured Wicks

Within vapor chambers, the wick structure serves the important role of returning liquid from the condensing end of the vapor chamber to the evaporating end of the vapor chamber via capillary action. The capillary pressure can be calculated using Eq. (3), which relates the liquid surface tension ( $\sigma$ ), contact angle of the liquid and solid material, in this case water/titanium ( $\theta$ ), and the effective pore radius ( $r_e$ ). As the effective pore radius decreases in size, the capillary pressure of the wick increases. However, with too small of a pore radius, the liquid inventory of the vapor chamber may not be enough to adequately wet the evaporator and dryout may occur. Therefore, the capillary pressure needs to be high enough to transport liquid across the longest path within the vapor chamber, but not so high as to reduce the heat transport capabilities of the vapor chamber.

$$\Delta P_c = \frac{2 \times \sigma \times \cos \theta}{r_e} \tag{3}$$

Due to the unique shape of the vapor chambers, additive manufacturing (AM) is the ideal option for fabrication. This presents the opportunity to finely control the wick design through additive manufacturing, ensuring adequate capillary pumping action and coverage of the wick on the internal structures of the vapor chamber. Lattice structures

are suitable for wick design, and several research efforts have described how to fabricate these structures using laser powder bed fusion (LPBF) for multifunctional heat exchangers,<sup>7</sup> as well as how to determine the effective pore radius for these structures.<sup>8</sup>

Common CAD software would be overloaded in modeling the wick structure within the designed vapor chamber due to the size and complexity of the wicks. Field-driven software is equipped to design such detailed structures, and so the topology software nTop was used for wick design. This software offers many options for wick lattices. Ten of these were selected for testing and are described in Table 2. In the design process, minimum feature thicknesses capable of being additively manufactured with fidelity dictated the size of the unit cells, and therefore the effective radius. The effective radius of each lattice was found using an internal tool to nTop. A coupon piece with each of the selected lattice structures was modeled and is shown in Figure 6. This test coupon is still in the process of fabrication and testing.

Table 2. Array of lattice unit cells, their effective radius, and resulti	aa aanillawu nuagguua
Table 2. Afray of fallice unit cens, their effective radius, and result	19 CADIHATY Dressure.

Wick #	Unit Cell	Effective Radius [mm]	Predicted Capillary Pressure [Pa]
1	Gyroid	0.399	258
2	Kelvin cell	1.189	87
3	Isotruss	0.267	386
4	Body centered cubic (BCC)	0.411	251
5	Octet	0.801	129
6	Face centered cubic (FCC)	0.655	157
7	Truncated cube	0.985	105
8	Truncated octahedron	0.382	270
9	Diamond	0.624	165
10	Simple Cubic	0.985	104

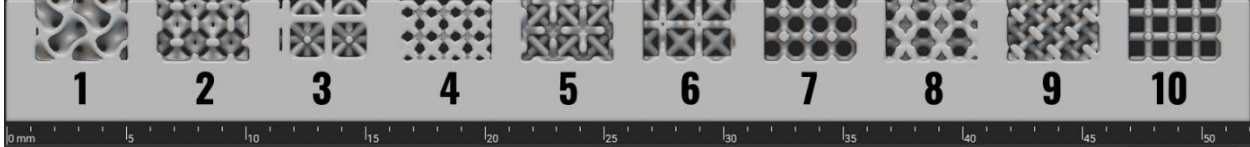


Figure 6. Cross-Section of Lattice Wick Coupon designed in nTop. The Numbered Labels correspond to data in Table 2.

To verify the design of the wicks, a wettability study will be performed on the printed coupon. The measured wicking height is directly related to the capillary pressure drawing the liquid up and the gravitational pressure head pushing the liquid down, as shown in Eq. (4).

$$H_{wick} = \frac{2 \times \sigma \times \cos \theta}{\rho_l \times g \times r_e} \tag{4}$$

Eq. (4) can be rewritten such that the actual capillary pressure of each wick design can be found from the measured wicking height and known constants.

### B. Thermal-Flow Analogy for Porous Media

To verify that the wick structure will adequately transport liquid across the vapor chamber, the thermal-flow analogy for porous media can be used to model flow through FEA. The thermal-flow analogy allows a conduction FEA simulation to model flow through a porous media, such as the wick structure. This is useful for complicated geometries that prohibit hand calculations. The two equations for thermal conduction and porous flow are shown in Eq. (5) and Eq. (6), respectively, and are of a similar form. The volumetric flowrate  $(\dot{V})$  can be equated to the total heat load  $(\dot{Q})$ . The thermal conductivity (k) can be equated to the wick permeability (k) divided by the liquid viscosity  $(\mu)$ , all of which are known quantities. Literature has provided a way to calculate the permeability for additively manufactured wicks comprised of the more common lattice structures.

$$\dot{V} = \frac{K}{\mu} \frac{A}{dx} \Delta P \tag{5}$$

$$\dot{Q}_{Analogy} = k \frac{A}{dx} \Delta T \tag{6}$$

The volumetric flow rate is determined by the heat flux profile shown in Eq. (7). Here, the latent heat ( $h_{fg}$ ) and density of the liquid ( $\rho$ ) are known, and the heat load is the actual heat load being applied to the vapor chamber.

$$\dot{V} = \frac{\dot{Q}_{Actual}}{h_{fg} \times \rho} \tag{7}$$

The largest concentric vapor chamber presents the most challenging path for liquid transport. As such, the wick volume for this vapor chamber was drafted in CAD then meshed in SolidWorks Simulation. For modeling the largest vapor chamber, only a quarter of the circle was modeled to reduce computational complexity. An additional inch was added to the height to account for the section of the vapor chambers where heaters will be attached externally to the zeolite bed. Of the possible wick selections from the nTop coupon, body centered cubic (BCC) was selected for modeling due to the wide availability of correlations for the permeability of the wick, and due to the lattice structure being an ideal candidate for AM. The volumetric flow rate determined from Eq. (7) is used as the total heat load on the bottom inch of the vapor chambers. This total heat load is treated as negative, as the flow of liquid as it evaporates is out of the wick structure. A constant temperature is set as the pressure boundary on the condensing surface of the wick. This pressure boundary is equal to the maximum possible capillary pressure of the wick, which is 251 Pa for the BCC wick. The resulting analysis, shown in Figure 7, determined that the maximum pressure drop across the wick was an acceptable 4 Pa. So long as the pressure difference does not exceed the capillary limit of the wick, the wick can provide adequate liquid flow to the evaporator from the condenser.

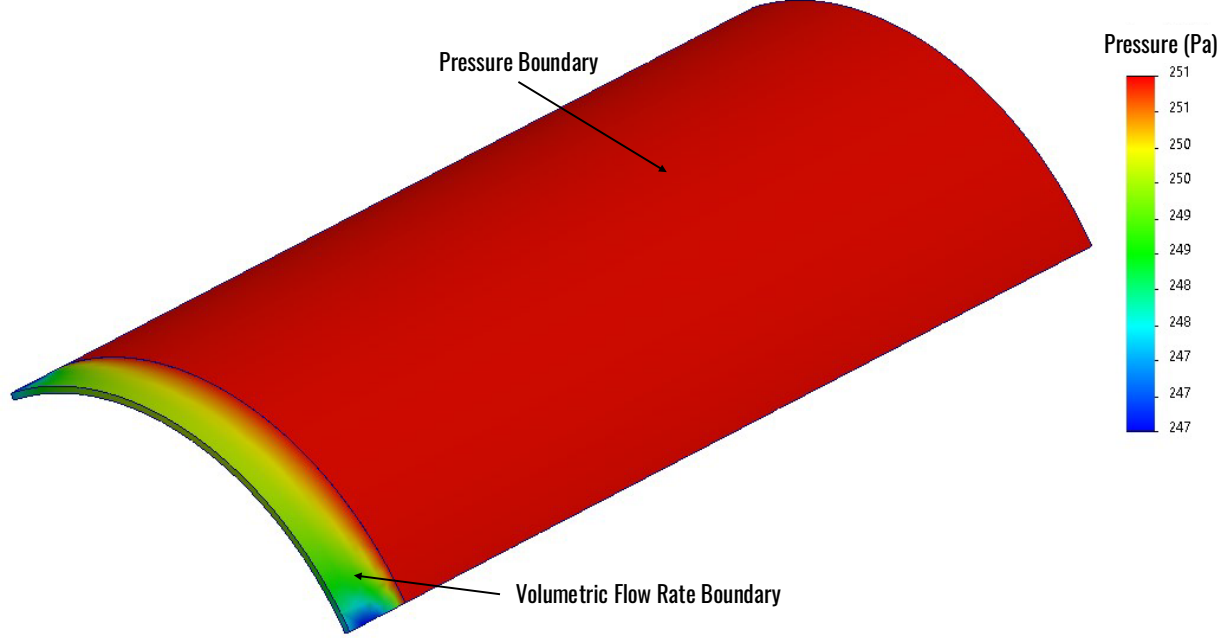


Figure 7. Porous Flow Analysis Results Showing Sufficient Capillary Pressure to Support Liquid Return Flow for a BCC Lattice Structure Wick.

To push the analysis to the limit, the same analysis was performed but with the pressure boundary present on only the very end of the vapor chamber wick. The results of this are shown in Figure 8, where the maximum pressure drop is found to be 40 Pa. This is an acceptable value, and so the BCC wick is acceptable as a wick structure for the concentric vapor chambers. Once the AM wick coupon is examined and a wick structure is selected for the printed full-scale model, this simulation will be updated to confirm that the capillary pressure is adequate.

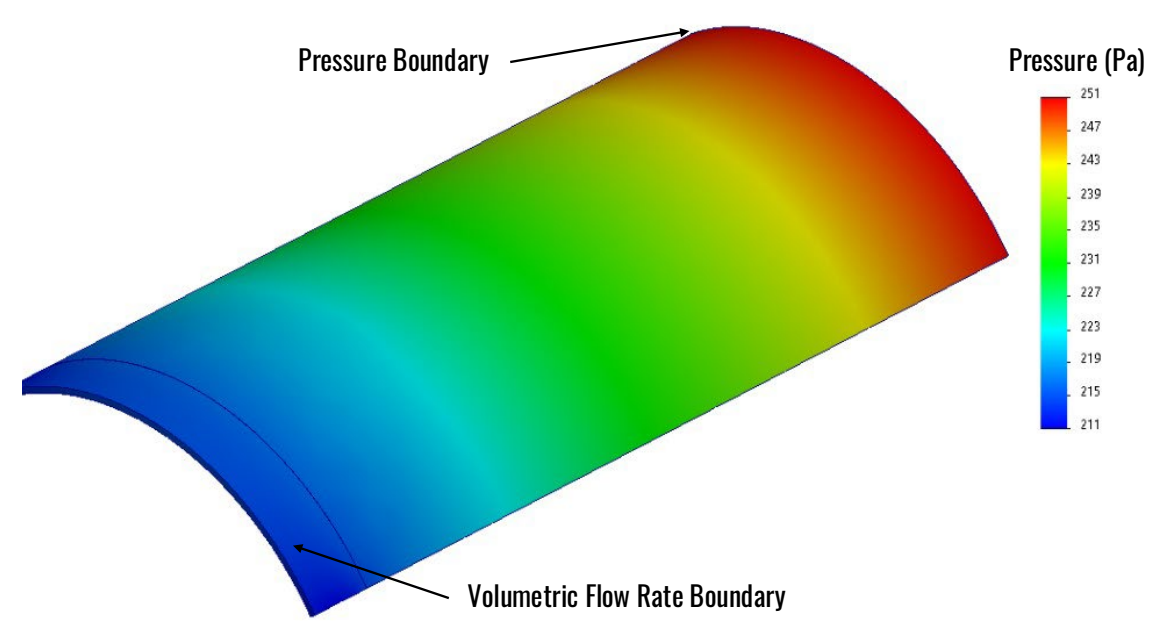


Figure 8. Porous Flow Analysis Results Showing Sufficient Capillary Pressure to Support Liquid Return Flow for a BCC Lattice Structure Wick for an Extreme Case.

## IV. Structural Study

Now that the thermal design of the vapor chambers has been determined, the design model must be made into a fabrication model. There are several design considerations that must go into designing for additive manufacturing, including the structural strength of the design. Vapor chambers contain both liquid and gas at saturation, and at the design temperature of 230 °C, the saturation pressure of water is 1553 kPa. This is much higher than ambient pressure, and so the vapor chambers must undergo a structural analysis to verify that the chambers can contain that pressure without rupture. The largest force experienced by a single vapor chamber will be found on the largest vapor chambers, with the largest surface area. A simple FEA pressure study was completed on the largest arc-shaped vapor chamber and is shown in terms of Factor of Safety (FOS) in Figure 9. The minimum FOS of the model was found to be 0.37, with the edges of the chamber found to be just above one. For space applications, a minimum FOS of 4 is preferred. This can be improved through the addition of targeted support structures to prevent the outward deformation of the chamber.

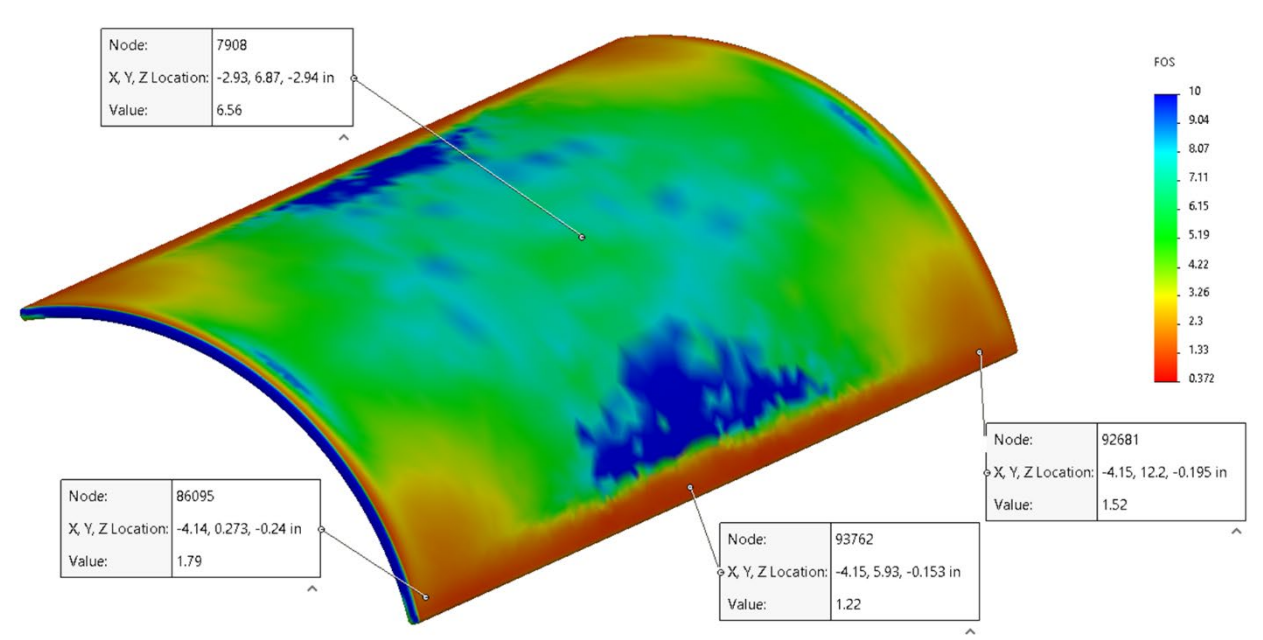


Figure 9. Factor of Safety Plot for Pressure Vessel Structural Study on Arc-Shaped Vapor Chamber. The color map was capped at a maximum of 10 to highlight the FOS gradient.

#### V. Conclusion

This paper offered a detailed methodology on approaching a unique thermal challenge found in CO<sub>2</sub> removal systems that use low-conductivity materials yet have high thermal demands. Concentric and arc-shaped vapor chambers look to be a promising solution due to their high degree of temperature control. The next steps in this program are to assess the wicks printed with designs generated from nTop. Once a wick design is selected, the final full-scale model for fabrication can be completed, and a structural analysis can be performed. Support structures, if needed, will then be added. The vapor chambers will then be additively manufactured and tested in a zeolite bed to confirm performance. For future works, the vapor chamber design will be adjusted as needed to meet industry and NASA standards for spaceflight hardware, such as the additive manufacturing requirements for spaceflight systems described in NASA-STD-6030.

## Acknowledgments

ACT would like to acknowledge the NASA SBIR program for financially supporting the project, and Tra-My Justine Richardson for her technical support and guidance as the technical monitor.

### References

<sup>1</sup>Gold, S., "The Survival Rule of 3 | Air, Shelter, Water, & Food," *Truprepper* [online journal], URL: <a href="https://trueprepper.com/survival-rule-of-3/">https://trueprepper.com/survival-rule-of-3/</a> [cited 17 May 2024].

<sup>2</sup>Knox, J. C., Coker, R. F., Huff, T. L., Gatens, R. L., & Miller, L. A. (2019). CO<sub>2</sub> Removal for the International Space Station – 4-Bed Molecular Sieve (4BMS) Flight Hardware Development (NASA Technical Report No. 20190030375). National Aeronautics and Space Administration. https://ntrs.nasa.gov/api/citations/20190030375/downloads/20190030375.pdf

<sup>3</sup>LeVan, M. Douglas, and Carta, Giorgio. *Adsorption and Ion Exchange*, in Perry's Chemical Engineers' Handbook, 9th Edition. McGraw-Hill, 2018. (Zeolite thermal conductivity and sorbent behavior in TSA/PSA)

<sup>4</sup>Cesarano, J. I., Anderson, T., Richardson, T.-M. J., and Bigham, S., "Recent Developments For Robocast Zeolitic Lattices For Reversible CO2 Sorbent Monoliths," 53rd International Conference on Environmental Systems, Louisville, KY, 2024.

<sup>5</sup>Myer, H. E., and Ellis, M. C., "Novel Vapor Chambers for Heating and Cooling of Advanced Sorption Systems," *52nd International Conference on Environmental Systems*, Calgary, Alberta, 2022.

<sup>6</sup>Seber, E., and Ellis, M. C.,"Development of Concentric Vapor Chambers for Heating and Cooling of Advanced Sorption Systems," *53rd International Conference on Environmental Systems*, Louisville, KY, 2024.

<sup>7</sup>Hasan, M., Elkholy, A., and M. Narvan, M., "Capillary performance of strut-based lattice wicks fabricated using laser powder bed fusion.," *International Communications in Heat and Mass Transfer.*, 159: 108227, 2024.

<sup>8</sup>Altschuh, P., Kunz, W., M. Bremerich, Reiter, A., Selzer, M., and Nestler, B., "Wicking in Porous Polymeric Membranes: Determination of an Effective Capillary Radius to Predict the Flow Behavior in Lateral Flow Assays," *Membranes (Basel)*, vol. 12, no. 7, 21 June 2022.

<sup>9</sup>nTopology Inc., "nTop," 2025. [online]. URL: <a href="https://www.ntop.com/">https://www.ntop.com/</a> [cited 3 April 2025].